CHEMMEDCHEM

DOI: 10.1002/cmdc.201000425

Benzyl and Naphthalene Methylphosphonic Acid Inhibitors of Autotaxin with Anti-invasive and Anti-metastatic Activity

Renuka Gupte,[a] Renukadevi Patil,[a] Jianxiong Liu,[b] Yaohong Wang,[b] Sue C. Lee,[b] Yuko Fujiwara,[b] James Fells,[b] Alyssa L. Bolen,[b] Karin Emmons-Thompson,[a] C. Ryan Yates,[a] Anjaih Siddam,[a] Nattapon Panupinthu,[c] Truc-Chi T. Pham,[d] Daniel L. Baker,[d] Abby L. Parrill,[d, e] Gordon B. Mills,[c] Gabor Tigyi,*[b] and Duane D. Miller*[a]

Autotaxin (ATX, NPP2) is a member of the nucleotide pyrophosphate phosphodiesterase enzyme family. ATX catalyzes the hydrolytic cleavage of lysophosphatidylcholine (LPC) by lysophospholipase D activity, which leads to generation of the growth-factor-like lipid mediator lysophosphatidic acid (LPA). ATX is highly upregulated in metastatic and chemotherapy-resistant carcinomas and represents a potential target to mediate cancer invasion and metastasis. Herein we report the synthesis and pharmacological characterization of ATX inhibitors based on the 4-tetradecanoylaminobenzylphosphonic acid scaffold, which was previously found to lack sufficient stability in cellular systems. The new 4-substituted benzylphosphonic acid and 6-substituted naphthalen-2-ylmethylphosphonic acid analogues block ATX activity with K_i values in the low micromolar to nanomolar range against FS3, LPC, and nucleotide substrates through a mixed-mode inhibition mechanism. None of the compounds tested inhibit the activity of related enzymes (NPP6 and NPP7). In addition, the compounds were evaluated as agonists or antagonists of seven LPA receptor (LPAR) subtypes. Analogues **22** and **30 b**, the two most potent ATX inhibitors, inhibit the invasion of MM1 hepatoma cells across murine mesothelial and human vascular endothelial monolayers in vitro in a dose-dependent manner. The average terminal half-life for compound **22** is 10 ± 5.4 h and it causes a long-lasting decrease in plasma LPA levels. Compounds **22** and **30 b** significantly decrease lung metastasis of B16-F10 syngeneic mouse melanoma in a post-inoculation treatment paradigm. The 4-substituted benzylphosphonic acids and 6-substituted naphthalen-2-ylmethylphosphonic acids described herein represent new lead compounds that effectively inhibit the ATX–LPA–LPAR axis both in vitro and in vivo.

Introduction

Autotaxin (ATX, NPP2) is member of the nucleotide pyrophosphate phosphodiesterase (NPP) enzyme family. ATX catalyzes the hydrolysis of lysophosphatidylcholine (LPC) through lysophospholipase D (LPLD) activity, which leads to generation of the growth-factor-like lipid mediator lysophosphatidic acid (LPA).[1,2] ATX is a 125 kDa glycoprotein, originally isolated from human melanoma cells, that stimulates tumor cell motility and has been implicated in metastatic and invasive properties, as well as chemotherapeutic resistance of many carcinomas.[3–12] NPP6 and NPP7 are the only other known NPP isoforms that use lysophospholipids as substrates. However, in contrast to ATX, NPP6 and NPP7 act as lysophospholipase C. NPP6 cleaves phosphocholine from LPC, sphingosylphosphorylcholine, and glycerophosphorylcholine to generate monoacylglycerol, sphingosine, and glycerol, respectively.[13] NPP7, also referred to as alkaline sphingomyelinase, hydrolyzes sphingomyelin to generate ceramide in the intestinal tract, but also cleaves phosphocholine from LPC and platelet-activating factor to generate monoacyl- and alkylacetylglycerols.[14,15]

ATX is required for normal development. Homozygous ATX knockout mice die in utero at day 9.5, coinciding with a period of vascular stabilization.[16,17] Likewise, ATX plays an important

[a] *R. Gupte, Dr. R. Patil, Dr. K. Emmons-Thompson, Prof. C. R. Yates, Dr. A. Siddam, Prof. D. D. Miller*
Department of Pharmaceutical Sciences, College of Pharmacy
University of Tennessee
Health Science Center, Memphis, TN 38163 (USA)
Fax: (+1) 901 448-3446
E-mail: dmiller@uthsc.edu

[b] *Dr. J. Liu, Dr. Y. Wang, Dr. S. C. Lee, Dr. Y. Fujiwara, J. Fells, Dr. A. L. Bolen, Prof. G. Tigyi*
Department of Physiology, College of Medicine
University of Tennessee
Health Science Center, Memphis, TN 38163 (USA)
Fax: (+1) 901 448-7126
E-mail: gtigyi@uthsc.edu

[c] *Dr. N. Panupinthu, Prof. G. B. Mills*
Department of Systems Biology
The University of Texas M. D. Anderson Cancer Center
Houston, TX 77054 (USA)

[d] *Dr. T.-C. T. Pham, Prof. D. L. Baker, Prof. A. L. Parrill*
Department of Chemistry, University of Memphis
Memphis, TN 38152 (USA)

[e] *Prof. A. L. Parrill*
Computational Research on Materials Institute
University of Memphis, Memphis, TN 38152 (USA)

Supporting information for this article is available on the WWW under http://dx.doi.org/10.1002/cmdc.201000425.

role in the development of the nervous system, as ATX knockout mice show defects in neural tube development.[18] LPA is a mitogen, motogen, and anti-apoptotic agent which provides survival advantages to carcinomas that use LPA in an autocrine or paracrine fashion. Ovarian cancer cells produce high levels of LPA.[19–21] Copy numbers increase in ovarian cancers in chromosomal region 8q24, which contains the genes that encode ATX and the Myc oncogene.[22] Euer et al. found that ATX is among the 40 most upregulated genes in highly metastatic cancers.[23] It was recently shown that ectopic expression of ATX in mice leads to mammary intraepithelial neoplasia, which develops into invasive and metastatic tumors.[11] ATX inhibits paclitaxel-induced apoptosis in breast cancer cells,[6] and LPA renders ovarian cancer cells resistant to cisplatin and adriamycin.[24] ATX is also overexpressed in patients with recurrent disease after prior chemotherapeutic treatment.[25] In a genome-wide siRNA screen, we identified ATX as a candidate drug-resistance gene in ovarian cancer.[7] We also showed that a lipid-like small-molecule inhibitor of ATX, carbacyclic phosphatidic acid, increases the sensitivity of resistant ovarian cancer cells to paclitaxel treatment.[7]

The ATX–LPA–LPAR axis is a promising therapeutic target for the management of cancer metastasis and therapeutic resistance. ATX shows feedback inhibition by its hydrolysis products LPA, cyclic phosphatidic acid, and sphingosine-1-phosphate (S1P).[26,27] Many initially identified ATX inhibitors are lipid-like substrate or product analogues.[28–35] The characteristics of these types of compounds limit their utility as potential lead compounds for drug development. Non-lipid ATX inhibitors have also been identified, but most of these compounds lack sufficient stability and characterization in tumor models.[30,36–41] Ferry and colleagues recently described an ATX inhibitor, 4-tetradecanoylaminobenzylphosphonic acid (S32826), that possesses nanomolar activity in vitro.[42] Unfortunately, S32826 failed to show activity in cellular and in vivo systems. We hypothesized that hydrolysis of the amide bond present in S32826 could be the reason for its instability and thus lack of activity in cellular systems.

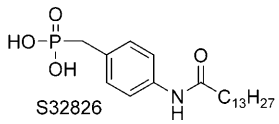

To overcome the presumed lack of stability of S32826, we designed analogues that are expected to be more stable than the parent compound. We generated a panel of analogues that inhibit ATX with potencies similar to that of S32826. These stabilized analogues inhibit ATX by a mixed-mode mechanism in vitro without any effect on the related lysophospholipid phosphodiesterases NPP6 and NPP7, or on LPAR. Two of these compounds, **22** and **30b**, inhibited ATX-dependent invasion of rat MM1 hepatoma cells of mesothelial cell and human umbilical cord vascular endothelial cell (HUVEC) monolayers in vitro. In addition, **22** and **30b** showed a profound decrease in lung foci in vivo using the B16-F10 syngeneic melanoma metastasis model in C57BL/6 mice. Based on these results, compounds **22** and **30b** represent promising leads for further synthetic improvement and also provide proof of principle that ATX inhibitors offer therapeutic utility in the control of cancer metastasis in vivo.

Results and Discussion

Synthesis

The synthesis of 4-(hexadecane-1-sulfonylamino)benzylphosphonic acid (**4**) is depicted in Scheme 1. Commercially available 1-hexadecanesulfonyl chloride (**2**) was added to a mixture of 4-aminobenzylphosphonic acid diethyl ester (**1**) and *N*,*N*-diisopropylethylamine in THF under reflux conditions to give compound **3**, which was deprotected with bromotrimethylsilane (TMSBr) followed by the addition of methanol under stirring for 30 min to afford compound **4**. The synthesis of compound **10** started with alkylation of 4-hydroxymethylphenol (**5**) (Scheme 2) using 1-bromotetradecane (**6**) in the presence of potassium carbonate and 18-crown-6 to furnish compound **7** followed by treatment with phosphorus tribromide to obtain **8** in 98% yield. The Michaelis–Arubuzov reaction[43] on compound **8** in trimethyl phosphate provided compound **9**, which was then deprotected using TMSBr in anhydrous acetonitrile to yield **10**.

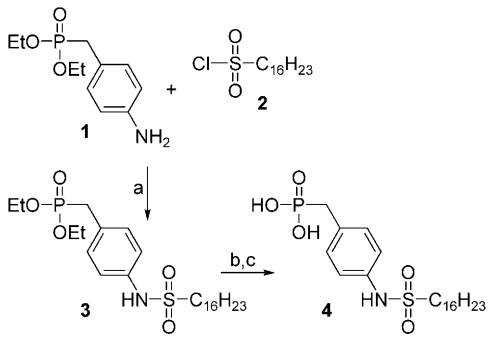

Scheme 1. *Reagents and conditions:* a) *N*,*N*-diisopropylethylamine, THF, reflux, 24 h; b) TMSBr, CH_3CN, reflux, 1 h; c) MeOH, RT, 30 min.

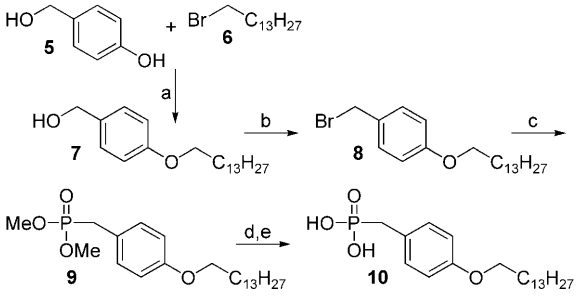

Scheme 2. *Reagents and conditions:* a) K_2CO_3, 18-crown-6, acetone, reflux, 16 h; b) PBr_3, Et_2O, RT, 30 min; c) $P(OMe)_3$, reflux, 18 h; d) TMSBr, CH_3CN, reflux, 1 h; e) MeOH, RT, 30 min.

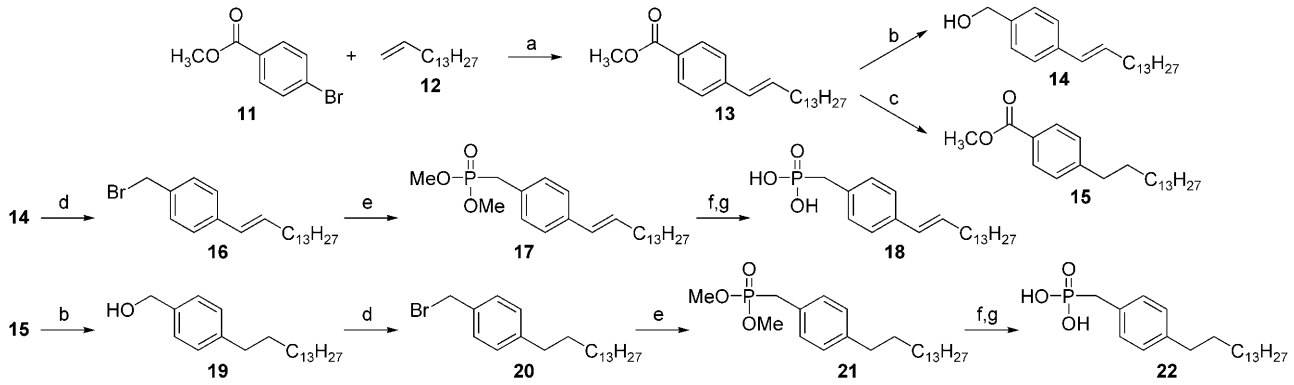

Scheme 3. *Reagents and conditions:* a) $Pd(OAc)_2$, Et_3N, DMF, reflux, 16 h; b) $LiAlH_4$, THF, 0 °C–RT, 4 h; c) H_2, Pd/C, MeOH, RT, 2 h; d) PBr_3, Et_2O, RT, 30 min; e) $P(OMe)_3$, reflux, 18 h; f) TMSBr, CH_3CN, reflux, 1 h; g) MeOH, RT, 30 min.

Scheme 3 illustrates the synthesis of (*E*)-4-(pentadec-1-enyl)-benzylphosphonic acid **(18)** and 4-pentadecylbenzylphosphonic acid **(22)**. (*E*)-Methyl-4-(pentadec-1-enyl)benzoate (**13**) was synthesized by the Heck coupling of **11** and **12** using palladium(II) acetate and triethylamine in anhydrous DMF. Compound **13** was reduced with lithium aluminum hydride in THF at 0 °C to room temperature to produce **14** and was also saturated under catalytic hydrogenation conditions to generate compound **15**. Bromination of compound **14** with phosphorus tribromide in diethyl ether gave **16**, which was then subjected to the Michaelis–Arubuzov reaction[43] using trimethylphosphite to get **17**. Compound **17** was treated with TMSBr in acetonitrile followed by the addition of methanol to furnish **18**. Compound **22** was synthesized by using the same approach starting from compound **15**.

The synthesis of 6-substituted naphthalen-2-ylmethylphosphonic acid analogues **(30a,b** and **34a,b)** was performed by using the same procedure described for the synthesis of compounds **18** and **22** (Scheme 4). We then focused our medicinal chemistry efforts on phosphomimetic functional groups; the phosphomimetics include compounds **37**, **41**, **42**, and **43** (Scheme 5). We started with the conversion of compound **19** into an aldehyde derivative **35** using pyridinium dichromate (PDC) in dichloromethane. The resulting aldehyde **35** was then

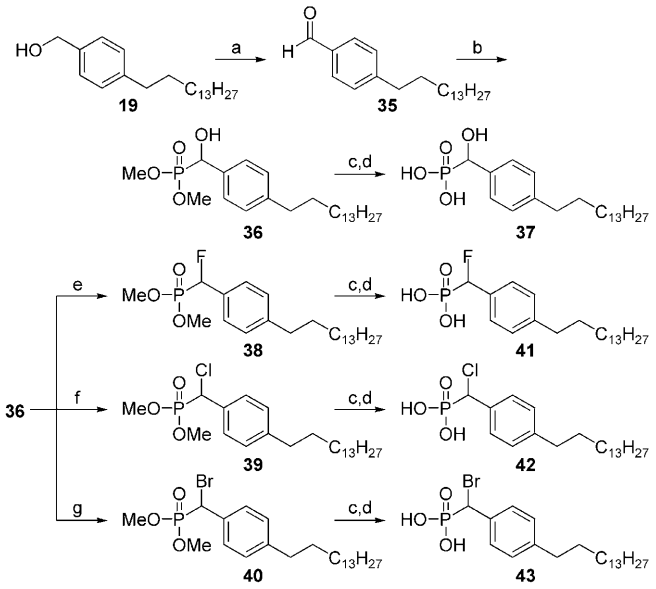

Scheme 5. *Reagents and conditions:* a) PDC, CH_2Cl_2, RT, 16 h; b) $HP(O)(OCH_3)_2$, Et_3N, 0 °C–RT, 4 h; c) TMSBr, CH_3CN, reflux, 1 h; d) MeOH, RT, 30 min; e) DAST, Et_2O, 0 °C–RT, 1 h; f) $SOCl_2$, CH_2Cl_2, reflux, 1 h; g) PBr_3, Et_2O, RT, 30 min.

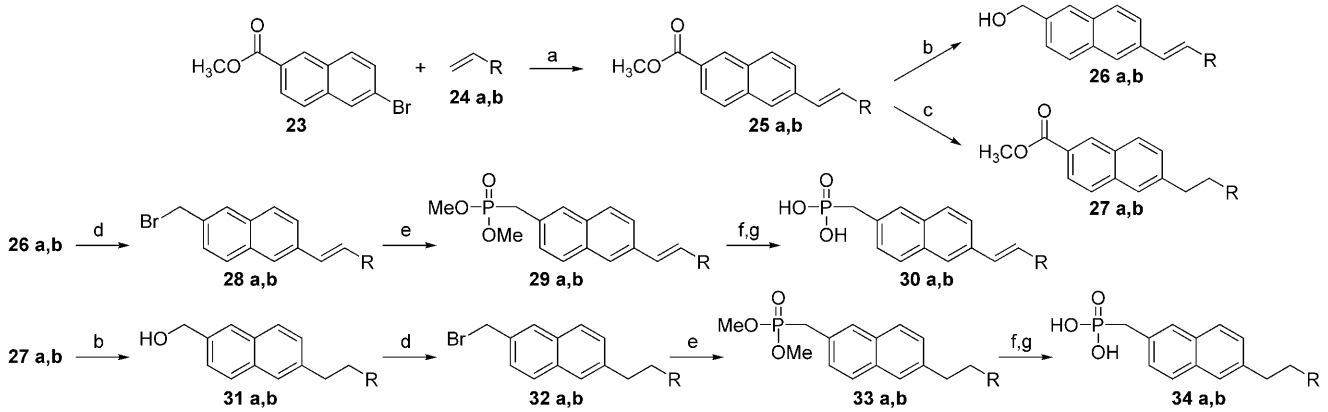

Scheme 4. *Reagents and conditions:* a) $Pd(OAc)_2$, Et_3N, DMF, reflux, 16 h; b) $LiAlH_4$, THF, 0 °C–RT, 4 h; c) H_2, Pd/C, MeOH, RT, 2 h; d) PBr_3, Et_2O, RT, 30 min; e) $P(OMe)_3$, reflux, 18 h; f) TMSBr, CH_3CN, reflux, 1 h; g) MeOH, RT, 30 min.

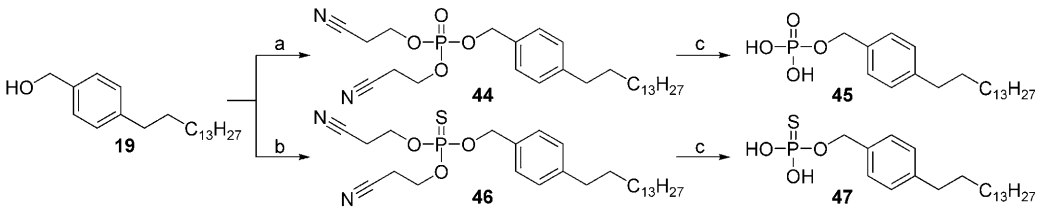

Scheme 6. *Reagents and conditions:* a) 1. bis(2-cyanoethyl)-*N*,*N*-diisopropylphosphoramidite, 1*H*-tetrazole, CH_2Cl_2, RT, 1 h, 2. 50% H_2O_2, RT, 1 h; b) 1. bis(2-cyanoethyl)-*N*,*N*-diisopropylphosphoramidite, 1*H*-tetrazole, CH_2Cl_2, RT, 1 h, 2. sulfur, reflux, 2 h; c) 1. KOH, MeOH, RT, 3 h, 2. dil HCl, RT, 3 h.

converted into the α-hydroxyphosphonate derivative **36** via the Pudovik reaction.[33,44] Compound **36** was deprotected with TMSBr to produce target compound **37**. Compound **36** was treated with diethylaminosulfur trifluoride (DAST) in Et_2O, $SOCl_2/CH_2Cl_2$, or PBr_3/Et_2O to obtain the desired compounds **38**, **39**, and **40**, respectively. Finally, compounds **38**, **39**, and **40** were treated with TMSBr followed by the addition of methanol to afford compounds **41**, **42**, and **43** in good yields.

The synthesis of target compounds **45** and **47** is outlined in Scheme 6. Compound **19** was treated with a mixture of 1*H*-tetrazole and bis(2-cyanoethyl)-*N*,*N*-diisopropylphosphoramidite in anhydrous dichloromethane followed by the addition of hydrogen peroxide to give the bis-cyanoethyl-protected fatty alcohol phosphate **44**. Removal of the cyanoethyl groups by treatment with methanolic potassium hydroxide followed by acidification furnished the phosphate **45**. Similarly, **19** was treated with a mixture of 1*H*-tetrazole and bis(2-cyanoethyl)-*N*,*N*-diisopropylphosphoramidite in anhydrous dichloromethane followed by reflux in the presence of elemental sulfur to give bis-cyanoethyl-protected fatty alcohol thiophosphate **46**, which, in turn, was treated with methanolic potassium hydroxide followed by acidification to yield the thiophosphate **47**.

Biological results

Effect of 4-substituted benzylphosphonic acid and 6-substituted naphthalene-2-ylmethylphosphonic acid derivatives on ATX and LPAR

The first level of testing was done with compounds at 10 μM added to recombinant human ATX and the FRET substrate FS3, each at 2 nM. After incubation for 2 h, the amount of FS3 hydrolyzed was measured, and residual ATX activity was expressed as a percentage of the vehicle-treated sample minus the autolysis of FS3 in the absence of ATX. In this assay, S32826 decreased the amount of FS3 hydrolyzed by 97% (Tables 1 and 2). Among the 4-substituted benzylphosphonic acid analogues, compound **22** showed 95% inhibition of FS3 hydrolysis (Table 1), whereas compound **30b** from the 6-substituted naphthalene-2-ylmethylphosphonic acid series decreased

Table 1. Characterization of benzylphosphonic acids at ATX, NPP6, and NPP7.[a]

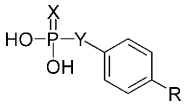

				ATX					NPP6	NPP7
Compd	X	Y	R	Activity [%][b]	IC_{50} [μM]	Mechanism[c]	K_i [μM]	K_i' [μM]	Activity [%][b]	Activity [%][b]
S32826	O	CH_2	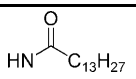	2.6	ND	ND	NA	NA	102.1	101.2
4	O	CH_2	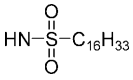	24.1	ND	ND	NA	NA	102.0	93.5
10	O	CH_2	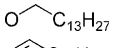	30.4	ND	ND	NA	NA	102.0	100.6
18	O	CH_2	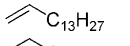	18.8	ND	ND	NA	NA	104.0	97.7
22	O	CH_2	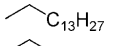	5.2	0.17	mixed	0.27	0.28	96.5	96.7
37	O	CHOH	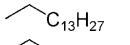	9.2	0.73	mixed	0.45	0.70	99.6	101.0
41	O	CHF	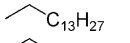	42.3	17.9	mixed	4.97	5.54	101.1	102.6
42	O	CHCl	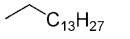	117.9	ND	ND	NA	NA	100.6	99.9
43	O	CHBr	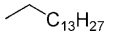	60.1	10.1	mixed	6.10	2.97	99.3	99.5
45	O	O–CH_2	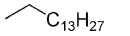	85.2	ND	ND	NA	NA	100.9	98.8
47	S	O–CH_2	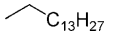	15.2	1.54	mixed	4.45	4.43	98.8	92.9

[a] ND: not determined; NA: not applicable, as the mechanism of inhibition was not determined. [b] Expressed as a percent of control at 10 μM. [c] Mechanism of inhibition.

FS3 hydrolysis by 83% (Table 2). Dose–response curves were generated with compounds S32836, **22**, and **30b** and compared with the feedback inhibition of the ATX product LPA (Figure 1). Each of these three compounds inhibited ATX in a dose-dependent manner.

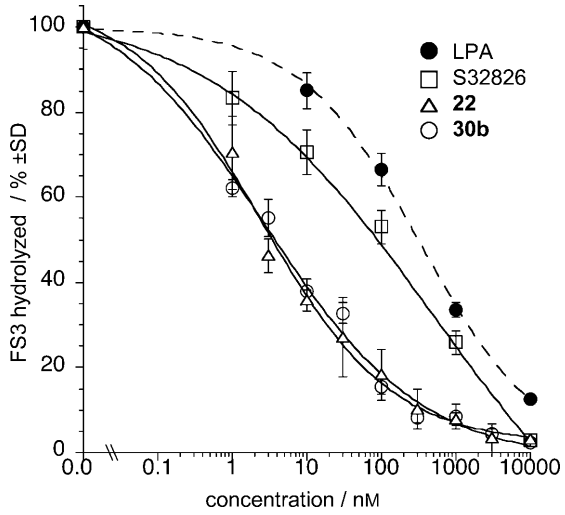

Figure 1. Inhibition of ATX-mediated hydrolysis of FS3 by LPA, S32826, **22**, or **30b**. ATX (2 nM) and FS3 (1 μM) were incubated in the presence of increasing concentrations of the inhibitors for 2 h, and the fluorescent product was measured and expressed as percent of FS3 hydrolysis by ATX in the presence of vehicle minus the autolysis of FS3 ($n=3\pm$SD).

Next we generated analogues of compounds **22** and **30b** and examined their inhibition of ATX. The modifications were either in the aliphatic chain, the linker of the phosphate moiety, or on the phosphate moiety itself (Table 1 and Table 2). The most effective analogues based on the single 10 μM dose inhibition assay were extensively characterized to determine IC_{50}, K_i, and K_i' values against ATX-mediated hydrolysis of FS3. Replacement of the amide with a sulfonamide (compound **4**) decreased potency. Introduction of an ether (in **10**) or alkene (in **18**) connecting the hydrocarbon chain to the benzyl ring decreased potency relative to the simple aliphatic chain. Linkage of the phosphate moiety in compound **45** through a methyl phosphonate decreased efficacy. However, converting the phosphate to a thiophosphate (compound **47**) in this scaffold increased efficacy 5.6-fold at 10 μM. α-Halogenation of the linker methyl group generally decreased potency of compounds **41**, **42**, and **43** relative to compound **22**. Insertion of an α-hydroxy group into the linker methylene increased the potency of this analogue, but it did not surpass that of compound **22**.

Modification of the side chain at position 6 of the naphthalene-2-ylmethylphosphonic acid scaffold showed that the 10-carbon side chain is more effective than the 11-carbon chain and that incorporation of an alkene has differential effects depending on the chain length (decreased efficacy of compound **30a** relative to **34a**, but increased efficacy of **30b** over **34b**). Analysis of the seven analogues showed that compound **22** in the benzylphosphonic acid series and compound **30b** in the naphthalene methylphosphonic acids are the most potent analogues with respect to ATX inhibition.

Because FS3 is not a natural substrate of ATX, we determined whether the inhibitors can also block LPA production from a fluorescent analogue of LPC (3-acyl-7-dimethylaminonaphtyl-1-LPC, ADMAN-LPC) and the hydrolysis of the nucleotide-like substrate *p*-nitrophenylthymidine 5′-monophosphate (pNP-TMP). Compound **22** and **30b** inhibited LPA production form ADMAN-LPC and hydrolysis of the pNP-TMP substrate (Figure 2). To determine the mechanism of ATX inhibition, K_i (affinity of the compound for free enzyme) and K_i' (affinity of the compound for the enzyme–substrate complex) values were determined by using simultaneous nonlinear fits of the Michaelis–Menten equations for competitive, uncompetitive, mixed-mode, and noncompetitive inhibition as we have previously described.[36,39,45] These experiments uniformly showed that these compounds display similar K_i and K_i' values which is consistent with a mixed-mode type mechanism of inhibition.

ATX inhibitors have been examined against other NPP family members.[29,36,37] NPP6 and NPP7 are the only NPP isoforms beside ATX that are known to use lysophospholipid phosphodiesters as substrates. Thus, specificity was addressed by determining the activity of NPP6 and NPP7 in the presence and absence of these analogues. None of the analogues tested blocked the activity of NPP6 or NPP7 by >10% at a single 10 μM dose (Tables 1 and 2).

Table 2. Characterization of naphtylphosphonic acids at ATX, NPP6, and NPP7.[a]

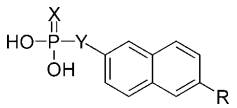

					ATX				NPP6	NPP7
Compd	X	Y	R	Activity [%][b]	IC_{50} [μM]	Mechanism[c]	K_i [μM]	K_i' [μM]	Activity [%][b]	Activity [%][b]
30a	O	CH_2	$C_{10}H_{21}$	61.3	ND	ND	NA	NA	103.1	100.0
30b	O	CH_2	$C_{11}H_{23}$	17.3	1.40	mixed	1.50	1.01	104.1	96.5
34a	O	CH_2	$C_{10}H_{21}$	19.9	ND	ND	NA	NA	101.0	98.8
34b	O	CH_2	$C_{11}H_{23}$	50.8	ND	ND	NA	NA	100.0	94.7

[a] ND: not determined; NA: not applicable, as the mechanism of inhibition was not determined. [b] Expressed as a percent of control at 10 μM. [c] Mechanism of inhibition.

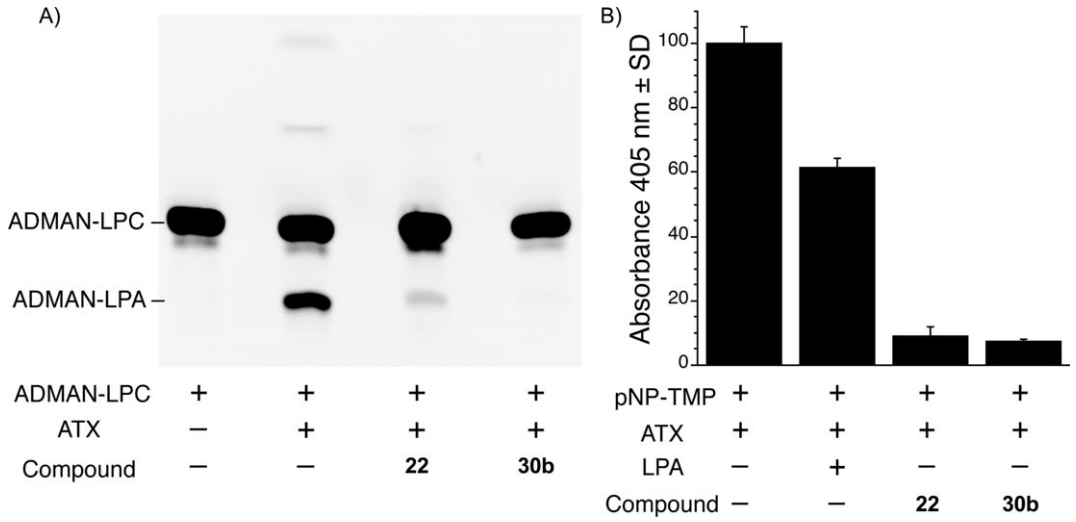

Figure 2. Inhibition of LPA production and pNP-TMP hydrolysis by compounds **22** and **30b**. A) Representative TLC image shows that compounds **22** and **30b** applied at 3 μM inhibit the hydrolysis of 0.5 μM ADMAN-LPC by 100 nM ATX. B) Compounds **22** and **30b** applied at 10 μM inhibit the hydrolysis of 5 mM pNP-TMP by 4 nM ATX more than the product LPA 18:1 applied at 10 μM.

Some inhibitors of ATX, including LPA phosphonates[28] and LPA bromophosphonates,[34] have been shown to inhibit ATX and block LPAR subtypes. LPA bromophosphonate (LPA-BP) was also shown to inhibit cancer metastasis and to decrease tumor size in mice.[34] For this reason, we examined whether the two leads **22** and **30b** can affect the activation of multiple LPA GPCR targets by using cell lines that overexpress individual LPA GPCRs coupled to Ca^{2+} mobilization, as we have previously described.[34] Analyses were carried out with test compounds (10 μM) alone or in combination with an EC_{50} concentration of LPA for the given receptor subtype to determine agonist and antagonist activity, respectively (Table 3).

Some of the compounds that showed >10% attenuation of the LPA response or activation >10% of LPA at a given receptor subtype at 10 μM were subjected to dose–response/inhibition experiments. Unexpectedly, compounds **45** and **47** were weak but full agonists at LPA_5 with EC_{50} values of 7.9 and 2.9 μM, respectively. Compound **47** is also a partial agonist at LPA_3 ($E_{max\,10\,\mu M}$ ~44% of maximal LPA response). Compound **45** caused a 50% decrease in the LPA_2 response when applied at 10 μM. Compound **33b** elicited a 33% activation of LPA_3 and a 17% activation at LPA_5 when applied at 10 μM. Likewise, compound **22** (10 μM) was a weak partial agonist at LPA_2 ($E_{max\,10\,\mu M}$ ~20%), whereas analogues **37** and **41** inhibited this receptor subtype by 28 and 26%, respectively. Based on these findings, we conclude that these analogues are poor ligands of the LPA GPCR tested, with the exception of compounds **45** and **47**, which are full agonists of LPA_5 albeit with low potency. At present, very few LPA_5-selective compounds have been described,[46] hence the identification of these two hits might serve as a starting point for a more comprehensive characterization of the structure–activity relationship of this receptor subtype.

ATX inhibitors block hepatocarcinoma invasion of mesothelial and HUVEC monolayers

Cancer metastasis is a complex process that cannot be accurately modeled in vitro. Models that use cell monolayers to monitor for the invasion of carcinoma cells come the closest to

Table 3. Activation of multiple LPA GPCR targets by various test compounds.[a]

Compd	RH7777 vector [$E_{max\,10\,\mu M}$][b]	LPA_1 [$E_{max\,10\,\mu M}$][b]	LPA_2 [$I_{max\,10\,\mu M}$][c]	LPA_3 [$E_{max\,10\,\mu M}$][b]	CHO vector [$E_{max\,10\,\mu M}$][b]	LPA_4	B103 vector [$E_{max\,10\,\mu M}$][b]	LPA_5 [$E_{max\,10\,\mu M}$][b]	LPA_5 [$I_{max\,10\,\mu M}$][c]
22	>1	NE	23	22	>1	NE	>3	NE	NE
30b	>6	NE	NE	33	>1	NE	>3	17	NE
37	>1	NE	28	NE	NE	NE	NE	NE	51
41	>3	NE	26	17	>5	NE	>1	NE	NE
43	>5	NE	NE	NE	>5	NE	>2	NE	NE
42	>15	ND	ND	ND	>74	ND	>32	ND	ND
45	>6	NE	50	13	>14	NE	>2	100[d]	NE
47	>7	10	NE	44	>14	NE	>3	100[e]	NE

[a] NE: no effect; ND: not definable due to effect on vector-transfected cells. [b] $E_{max\,10\,\mu M}$: maximal response at 10 μM relative to the maximal response to either ATP in vector-transfected cells or to LPA in LPAR-expressing cells. [c] $I_{max\,10\,\mu M}$: maximal inhibition of the ~EC_{75} LPA response caused by the compound applied at 10 μM. [d] EC_{50} = 7.9 μM. [e] EC_{50} = 2.9 μM.

the situation in vivo.[47–50] For this we used two different cell monolayers, mouse mesothelium and human umbilical vein endothelial cell (HUVEC), to examine the role of ATX in the invasion of MM1 hepatocarcinoma cells. The mesothelial monolayer is an accepted model for invasion of body cavities lined by serous cells, whereas the HUVEC monolayer is considered to be an in vitro model of hematogenous invasion of carcinomas.

First we determined if exposure to compounds **22**, **30b**, and the combined ATX inhibitor LPAR pan-antagonist compound LPA-BP[34] causes toxicity in vitro. We exposed the cells of the mesothelium monolayer or the MM1 cell line to these compounds (10 μM) dissolved in 1% DMSO for 20 h and examined cell viability with the trypan blue dye-exclusion assay. Neither compound caused a decrease in cell viability relative to the vehicle, and all viabilities were $>93\%$.

The mesothelial cells and HUVECs of the monolayer and the invading MM1 cells express different levels of ATX (Figure 3A–C). Quantitative real-time PCR performed with mRNA isolated from MM1, mesothelium, and HUVECs showed that the primary source of ATX are MM1 cells, as the other two cell types show very low expression. MM1 cells showed robust expression of transcripts encoding the P2Y family of LPARs and LPA_2 in the EDG receptor subfamily. In mesothelial cells LPA_2 is the predominant receptor, whereas in HUVECs it is the LPA_5 receptor.

Addition of LPC to the co-culture increases invasion in a dose-dependent manner (Figure 3D). We hypothesized that inhibition of ATX by our two lead compounds should attenuate LPA production in situ and decrease invasion of MM1 carcinoma cells through the mesothelial and HUVEC monolayers. Compounds **22** and **30b** were applied with or without LPC to the co-cultures, and the number of invading cells was quantified after 20–24 h of co-culture (Figure 3E). Both compounds inhibit MM1 cell invasion, reaching complete inhibition of LPA and likely ATX-dependent invasion above 3 μM. The two compounds were also tested for their ability to inhibit MM1 cell invasion of HUVEC monolayers (Figure 3F). Similarly to that observed for the invasion of murine mesothelial monolayers, compounds **22** and **30b** dose-dependently inhibited the LPC-dependent invasion of the HUVEC monolayer, whereas the compounds alone did not decrease the basal rate of invasion. We conducted similar experiments with rat microvascular cell monolayers and found similar inhibition with **22** and **30b**, although the number of invading cells per field was considerably lower than that in HUVEC or mesothelial monolayers (data not shown). These results provide evidence that the inhibition of ATX in situ can fully inhibit LPC-dependent invasion of carcinoma cells, suggesting the potential applicability of these compounds in animal models of carcinoma metastasis.

Pharmacokinetic characterization of compound 22

Because of the slightly higher potency of compound **22** as an ATX inhibitor, we selected this analogue for preliminary pharmacokinetic characterization. The time-dependent plasma concentration profile of compound **22** declined bi-exponentially, exhibiting initial distribution and terminal elimination phases (Figure 4). Non-compartmental analysis following intravenous administration showed that the volume of distribution (V_d) for compound **22** was 3.9 L kg^{-1}, and the clearance was estimated to be 8.6 ± 0.5 mL min^{-1} kg^{-1}. The average terminal half-life for compound **22** was 10 ± 5.4 h, with a mean plasma residence time of 7.6 ± 0.5 h. LPA levels were monitored simultaneously for the 16:0, 18:1, 18:2, and 20:4 acyl species and showed similar changes regardless of the fatty acyl chain length. Plasma LPA levels showed a rapid decrease with a nadir at 60 min followed by a transient rise at 120 min and second decrease reaching a minimum in the 480 min sample. LPA levels remained depressed at ~50% of the pretreatment level in the 1440 min sample, the longest sampling time included in the study. These results indicate a long-lasting decrease in plasma LPA that appears to be consistent with the 10 h $t_{1/2}$ value of this compound. Of note is a confounding factor that at 2 h, heparin (50 IU) was injected to keep the cannulas open, and this may have affected plasma LPA levels. Furthermore, these results may not be reflective of the levels following intraperitoneal administration used in the murine metastasis model. Further experiments are needed to characterize the pharmacokinetic properties of compound **22** and other analogues using different routes of administration. It is important to recognize that plasma LPA levels are not likely to be indicative of the LPA level in the tumor microenvironment as supported by the lack of elevation in LPA or ATX activity in different cancers, with the exception of follicular lymphoma.[8,19,41,51,52]

ATX inhibitors decrease B16 melanoma metastasis in vivo

We conducted an acute toxicity study with compound **22** by exposing Swiss mice to 1, 10, and 30 mg kg^{-1} day^{-1} doses for 10 days. We found no noticeable change in animal behavior within 1 h after injection, or weight loss. No death was detected in any of the groups. Necropsy conducted on day 14 showed no noticeable organ damage, with the exception of adhesions and splenomegaly in three mice in the group receiving the highest dose. We conclude that the non-observable adverse effect level of compound **22** is >10 mg kg^{-1}.

Inhibitors of ATX have been shown to decrease tumor metastasis in various animal models.[31,34] Here we applied the syngeneic B16-F10 mouse melanoma model of hematogenous lung metastasis in C57BL/6 mice that we previously showed responds to inhibitors of ATX.[31] C57BL/6 mice were inoculated with B16-F10 melanoma cells via the tail vein; 30 min later, the mice were treated with either of the two lead compounds (0.5 mg kg^{-1} day^{-1}) or vehicle (PBS with 1% DMSO) via the intraperitoneal route for an additional 10 days. As a positive control, we also applied LPA-BP, which we showed previously to inhibit the metastasis of breast and colon cancers in xenograft models.[34,53] On day 21 the animals were sacrificed and the lungs were isolated; metastatic nodules in the lungs were then quantified. In this metastasis model, compounds **22** and **30b** significantly decreased the number of metastatic foci, and their efficacy at this dose was similar to that of LPA-BP (Figure 5A and B).

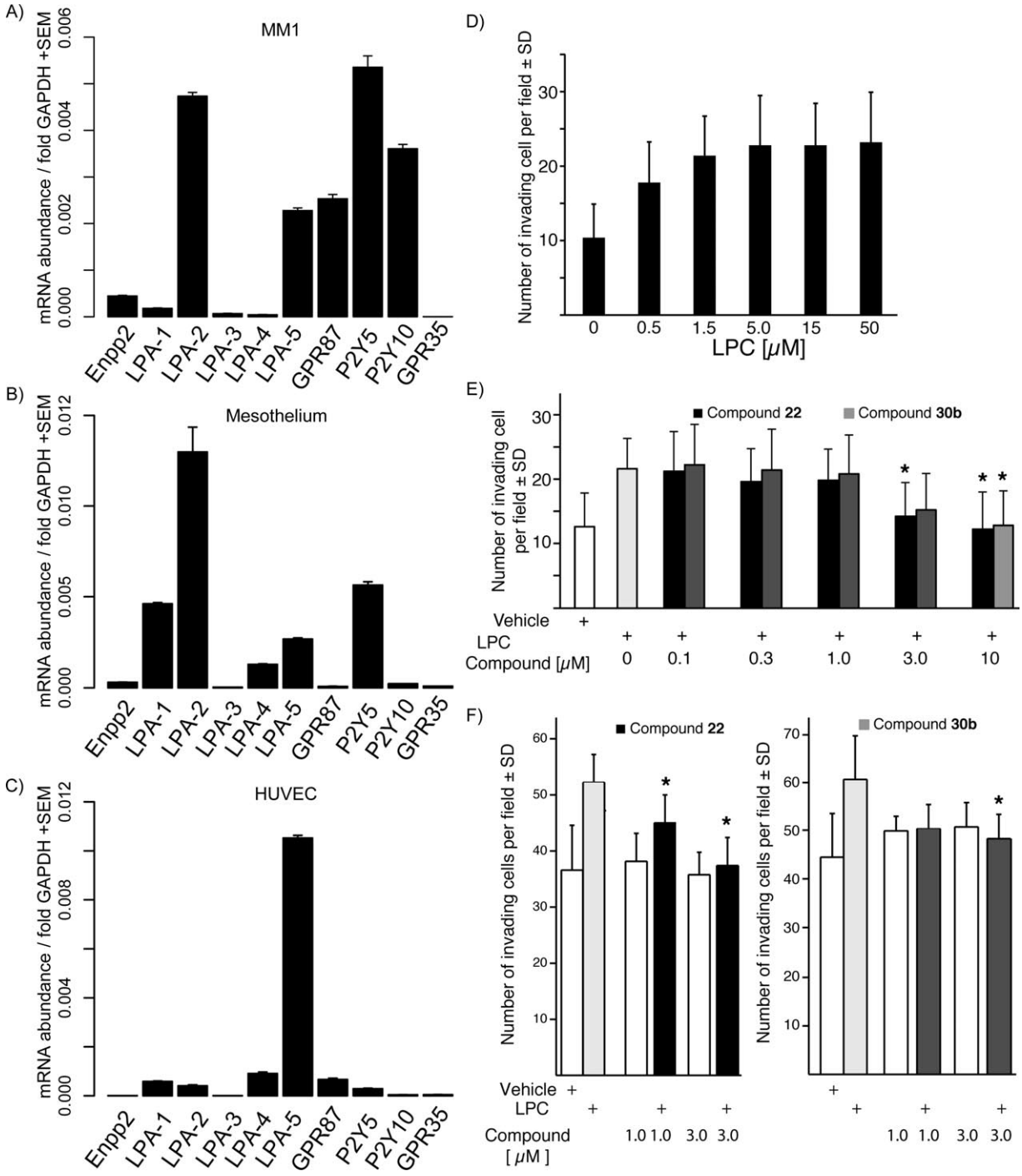

Figure 3. Profiling of LPAR and ATX transcripts in A) MM1, B) mouse mesothelial, and C) HUVECs using quantitative real-time PCR. D) LPC dose-dependently increases the invasion of mesothelial monolayers by MM1 cells. E) Compounds **22** and **30 b** dose-dependently inhibit the invasion of mesothelial monolayers induced by LPC (1.5 μM) that is decreased to the level of control at and above 3 μM. F) Compounds **22** and **30 b** block LPC-induced but do not alter the basal rate of invasion of HUVECs.

In this study we provide evidence for the potential therapeutic utility of ATX inhibitors derived from the benzylphosphonic acid scaffold. We have modified and expanded this scaffold to 6-substituted naphthalene-methylphosphonic acid derivatives that are also effective inhibitors of ATX. Our limited structure–activity analysis showed that some of these compounds are high-potency inhibitors of ATX without significant effects on LPA GPCR in the nanomolar and low micromolar range. Unlike the parent compound S32826 that lacks activity in cellular assays,[42] these novel analogues show strong inhibition of ATX-mediated tumor cell invasion of mesothelial and endothelial cell monolayers and are as effective in vivo as the previously reported dual-action ATX inhibitor and LPA GPCR antagonist LPA-BP.[31,34,53]

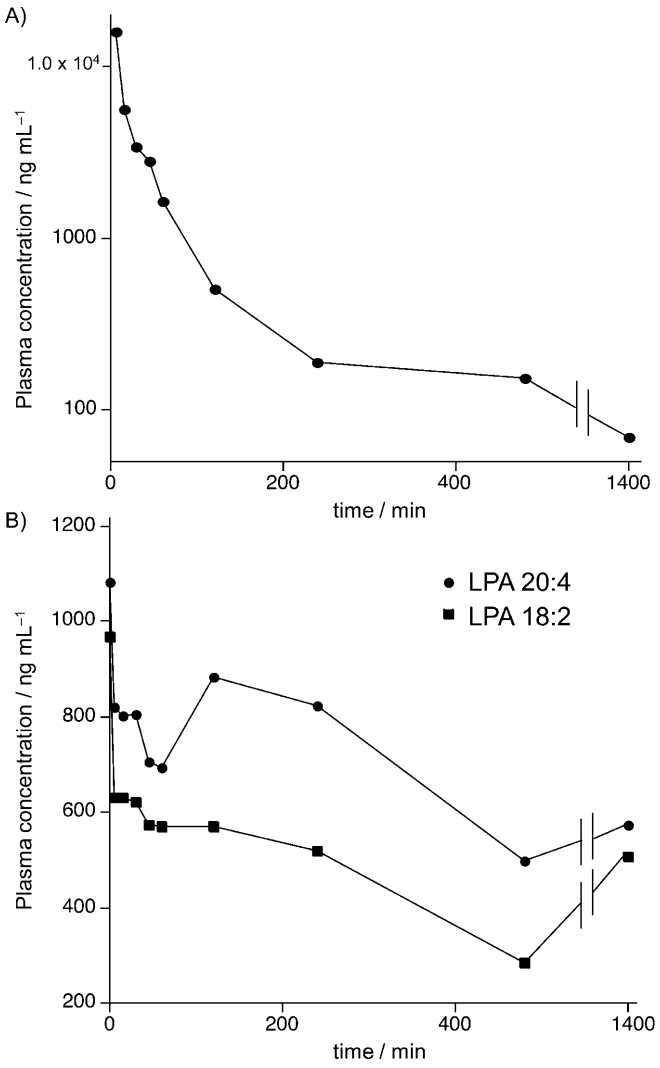

Figure 4. Plasma level of A) compound **22** and B) two LPA species after i.v. administration of a single dose at 5.8 mg kg^{-1}. Note that compound **22** has a relatively long half-life calculated at 10.5 h, plasma mean residence time (456 ± 33 min), and LPA 18:2 and 20:4 remain depressed over the 24 h duration of the study.

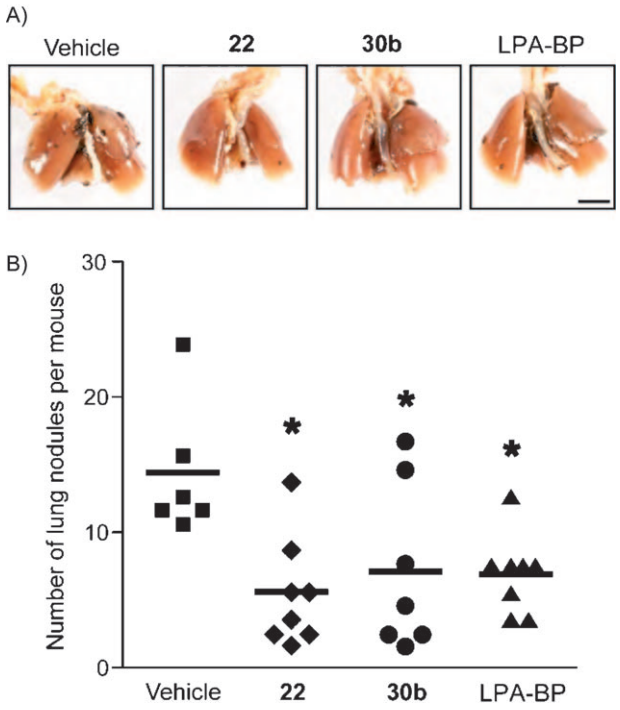

Figure 5. Effect of compounds **22**, **30 b**, and LPA-BP on the lung metastasis of B16-F10 melanoma. A) Representative lungs taken from the treatment groups. B) Lung nodule counts in the treatment groups; *$p < 0.05$ relative to vehicle.

There is increasing interest in the development of ATX inhibitors to control the tumor-promoting and pro-inflammatory roles of LPA.[29,30,34,36–39,54] Carbacyclic phosphatidic acid was the first ATX inhibitor scaffold explored to control carcinoma invasion and metastasis in vivo.[31] Carbacyclic phosphatidic acid inhibits ATX without activating LPA_{1-4}. However, these compounds activate LPA_5, and this complicates their utility.[46] Subsequently, the sn-1 or sn-2 hydroxy groups of LPA have been replaced by fluorine, difluoromethyl, difluoroethyl, *O*-methyl, or *O*-hydroxyethoxy groups to give non-migrating LPA analogues that resist acyltransferases.[55] Some of these compounds, including LPA-BP, have been found to possess dual action by inhibiting ATX and LPA GPCR.[34] LPA-BP inhibited breast cancer metastasis and tumor growth in vivo.[34] Several new ATX inhibitor scaffolds have been reported recently;[29,30,36–39,54] however, these compounds have not been evaluated against other members of the NPP family and were not explored for their ability to control invasion and/or metastasis. Our study provides initial proof of principle that ATX inhibitors are capable of controlling cancer metastasis in vivo; it also validates the monolayer invasion assay as a valuable cell-based screen for anti-metastatic compounds.

The preclinical screening template consisting of assays for the activity of analogues against ATX, followed by some related NPP isoforms, LPA GPCR, monolayer invasion assays, and then followed by the syngeneic animal metastasis model offers a comprehensive stepwise protocol for the identification of ATX inhibitors with utility to control tumor progression. Given the relatively short half-life of ATX[56] and the high rate of LPA turnover in vivo,[30] we foresee the need of compounds with long plasma half-lives and broad tissue distribution to control the constitutive production of ATX and the generation of LPA. The data presented herein, derived from cellular and in vivo experiments, suggest that further modification of the benzyl- and naphthylphosphonic acid scaffolds might yield even more suitable derivatives for the control of carcinoma metastasis. Pharmacokinetic profiling of other analogues will be a crucial step in further evaluation and preclinical development of ATX inhibitors for the identification of scaffolds that exert long-term inhibition of ATX in the tumor microenvironment.

Conclusions

Two autotaxin inhibitors, **22** and **30 b**, were identified to be potent and stable in in vivo models. All of the compounds syn-

thesized were specific for NPP2/ATX. The mode of enzyme inhibition for the most potent compounds was determined and was found to be mixed. The fact that the ATX inhibitors block hepatocarcinoma invasion of mesothelial and HUVEC monolayers lends evidence that the inhibition of ATX in situ can fully inhibit LPC-dependent invasion of carcinoma cells. This signifies the potential applicability of our compounds in animal models of carcinoma metastasis. Compounds **22** and **30b** have shown outstanding in vivo profiles by decreasing the lung metastases of B16-F10 syngeneic mouse melanoma in a post-inoculation treatment model.

Experimental Section

Chemistry

All starting materials, reagents, and solvents were obtained from commercial suppliers and were used without further purification. Reactions were performed under an inert atmosphere of N_2 unless otherwise specified. Routine thin-layer chromatography (TLC) was performed on silica gel plates (Analtech Inc., 250 μm). Flash chromatography was conducted on silica gel (Merck, grade 60, 230–400 mesh). ^{1}H NMR spectra were recorded on a Bruker ARX 300 spectrometer (300 MHz) or Varian spectrometer (500 MHz) using [D_6]DMSO and $CDCl_3$ as solvents, and spectral data were consistent with assigned structures. Chemical shift values (δ) are reported in ppm, coupling constants (J) are given in Hz, and splitting patterns are designated as follows: s, singlet; d, doublet; t, triplet; q, quartet; m, multiplet. MS data were collected on a Bruker ESQUIRE electrospray/ion-trap instrument in the positive and negative modes. High-resolution MS data were obtained using a Micromass Q-TOF2 mass spectrometer. Elemental analyses (C, H, N) were performed by Atlantic Microlab Inc. (Norcross, GA, USA), and results are within ±0.4% of the theoretical values for the formula given.

General procedure for the synthesis of phosphonic acid analogues (compounds 4, 10, 18, 22, 30a, 30b, 34a, 34b, 37, 41, 42 and 43) (GP 1): To a suspension of phosphonate derivative (1 equiv) in anhydrous CH_3CN, TMSBr (2.5 equiv) was added, and the reaction mixture was held at reflux for 1 h. The CH_3CN was then evaporated under reduced pressure, and MeOH was added to the residue and stirred for 30 min at RT. The desired product was obtained in good yield after filtration of the MeOH solution as a white solid.

4-Pentadecylbenzylphosphonic acid (22): Yield (0.153 g, 53%); ^{1}H NMR (500 MHz, [D_6]DMSO): δ = 7.14–7.06 overlapping protons (m, 4H), 2.91 (d, J = 20 Hz, 2H), 1.52 (m, 2H), 1.26 (m, 2H), 1.15 (s, 24H), 0.85 ppm (t, J = 6.5 Hz, 3H); ^{13}C NMR (500 MHz, [D_6]DMSO): δ = 140.2, 131.6, 129.8, 128.4, 38.1, 35.1, 31.8, 29.5, 29.3, 29.2, 22.6, 14.2 ppm; MS (ESI) m/z 381.0 $[M-H]^-$; Anal. calcd for $C_{22}H_{39}O_3P$: C 69.08, H 10.28, found: C 69.33, H 10.52.

General procedure for the synthesis of compounds 8, 16, 20, 28a, 28b, 32a, 32b, and 40 (GP 2): PBr_3 (0.3 equiv) was added slowly under stirring to a solution of alcohol derivative (1 equiv) in anhydrous CH_2Cl_2 at 0 °C. The reaction mixture was stirred at RT for 1 h and the formation of the product was monitored by TLC. H_2O was added at 0 °C to quench the reaction, extracted from CH_2Cl_2, and dried over $MgSO_4$. The product mass was confirmed by MS and the residue was carried on to the next step without further purification.

1-Bromomethyl-4-pentadecylbenzene (20): MS (ESI) m/z 380 $[M-H]^-$.

General procedure for the synthesis of compounds 9, 17, 21, 29a, 29b, 33a, and 33b (GP 3): Trimethylphosphite (9 equiv) was added to dry bromide derivative (1 equiv) at RT, and the mixture was held at reflux for 18 h. The trimethylphosphite was evaporated under high vacuum overnight, and the crude residue was purified by column chromatography ($CHCl_3$/MeOH 3:1) to give pure compound in quantitative yield.

Dimethyl-4-pentadecylbenzylphosphonate (21): ^{1}H NMR (300 MHz, $CDCl_3$): δ = 7.40–7.00 overlapping protons (m, 4H), 3.66–3.63 (d, J = 15 Hz, 6H), 3.2 (d, J = 11 Hz, 2H), 2.6 (m, 2H), 1.6 (m, 2H), 1.2 (s, 24H), 0.90 ppm (t, J = 7.5 Hz, 3H); MS (ESI) m/z 433 $[M+Na]^+$.

General procedure for the synthesis of compounds 13, 25a, and 25b (GP 4): To a mixture of aryl bromide derivative (1 equiv), palladium(II) acetate (5 mol%), and Et_3N (1 equiv) in anhydrous DMF was added substituted alkene (1 equiv) successively. The reaction mixture was held at reflux for 16 h, filtered on a bed of Celite and extracted with EtOAc and H_2O. The compound was purified by flash column chromatography using EtOAc and hexane (1:2).

(*E*)-Methyl-6-(dodec-1-enyl)-2-naphthoate (25a): ^{1}H NMR (300 MHz, [D_6]DMSO): δ = 8.58–7.77 overlapping protons (6H), 6.65–6.52 (m, 1H), 5.70–5.20 (m, 1H), 3.91–3.90 (s, 3H), 2.10–1.80 (m, 2H), 1.76–1.55 (m, 2H), 1.21 (s, 14H), 0.86 ppm (t, J = 5.1 Hz, 3H); MS (ESI) m/z 375.3 $[M+Na]^+$.

General procedure for the synthesis of compounds 14, 19, 26a, 26b, 31a, and 31b (GP 5): Anhydrous THF was added to $LiAlH_4$ (3 equiv) and stirred for 5 min. To this, a solution of corresponding methyl ester (1 equiv) in THF was added, and the mixture was stirred at RT for 4 h. The reaction mixture was cooled to 0 °C, and saturated Na_2SO_4 was added dropwise to the mixture. The product was then extracted with EtOAc, and the crude product was purified using flash column chromatography which was eluted with EtOAc and hexane mixture (1:1).

(*E*)-6-(Dodec-1-enyl)naphthalen-2-ylmethanol (26a): ^{1}H NMR (300 MHz, $CDCl_3$): δ = 7.90–7.30 overlapping protons (6H), 6.60–6.30 (m, 1H), 5.60–5.40 (m, 1H), 4.81 (s, 2H), 2.35–2.26 (m, 2H), 1.6–1.47 (m, 2H), 1.27 (s, 14H), 0.9 ppm (t, J = 4.8 Hz, 3H); MS (ESI) m/z 347.3 $[M+Na]^+$.

General procedure for the synthesis of compounds 15, 27a, and 27b (GP 6): To a solution of the corresponding alkene of the methyl ester derivative (1 equiv) in MeOH was added a catalytic amount of $Pd(OH)_2$/C, and the mixture was stirred at RT for 2 h using a catalytic amount of H_2 gas. The completion of reaction was monitored by TLC, and the reaction mixture was filtered on a bed of Celite. The filtrate was evaporated, product mass was confirmed by MS, and the crude residue was directly used for next step.

6-Dodecylnaphthalene-2-carboxylic acid methyl ester (27a): MS (ESI) m/z 355 $[M+H]^+$.

Biology

Lysophosphatidic acid (18:1), LPC 18:1, and S1P were purchased from Avanti Polar Lipids (Alabaster, AL, USA). For calcium mobilization assays, LPA, S1P, and the test compounds were prepared as 1 mM stock solutions in phosphate-buffered saline (PBS) in an equimolar complex with charcoal-stripped, fatty acid free bovine serum albumin (BSA; Sigma, St. Louis, MO, USA). The fluorescent

ATX substrate FS3 was purchased from Echelon Biosciences (Salt Lake City, UT, USA).

Autotaxin inhibition assays

As the first level of screen, recombinant-ATX (50 μL, 2 nM final concentration) in assay buffer [Tris 50 mM, NaCl 140 mM, KCl 5 mM, $CaCl_2$ 1 mM, $MgCl_2$ 1 mM (pH 8.0)] was mixed with 25 μL FS3 (Echelon Biosciences Inc., Salt lake city, UT, USA; final concentration 1 μM) and 25 μL test compound dissolved in assay buffer with 40 μM BSA in 96-well Costar black-well plates. FS3 fluorescence ($\lambda_{ex}=485$ nm, $\lambda_{em}=538$ nm) was monitored with a Flex Station II (Molecular Devices, Sunnyvale, CA, USA) for 2 h incubation at 37 °C. The differences between 0 and 120 min were calculated individually and normalized to vehicle control. The mean ±SD of triplicate samples was expressed as percentage of ATX activity. The ATX activity in the presence of the test compounds was compared with vehicle using Student's *t*-test, and $p<0.05$ was considered significant.

The second level of screen was aimed at determining the inhibition of ATX activity against LPC substrate. We used the fluorescent analogue ADMAN-LPC to measure the inhibition of LPA production as previously reported.[31] ADMAN-LPC at a final concentration of 0.5 μM was mixed with or without the test compound at 3 μM and 100 nM ATX. The reaction was incubated at 37 °C for 4 h, and lipids were extracted and separated by silica gel 60 TLC plates (Merck) using $CHCl_3$/MeOH/NH_4OH (60:35:8 *v*/*v*/*v*). Fluorescent LPC and LPA species were visualized in a Photodyne UV imager using the TotalLab100 software.

The third level of screen used the nucleotide-like substrate pNP-TMP (Sigma–Aldrich).[31] The assay contained 4 nM ATX, 5 mM pNP-TMP, and vehicle with or without the test compound (10 μM), all dissolved in 60 μL assay buffer. The assay was carried out in 96-well, half-area plates (Corning Inc., Corning, NY, USA) at 37 °C in a BioTek Synergy-2 plate reader (BioTek, Winooski, VT, USA) with absorbance monitoring at $\lambda=405$ nM.

Determination of the mechanism of autotaxin inhibition

The mechanism of ATX inhibition was determined with recombinant purified human ATX and FS3, as recently described.[36,37,39] Final ATX and FS3 concentrations were 8.3 and 1 μM, respectively, in assay buffer containing 15 μM fatty acid free BSA. To calculate IC_{50}, full dose responses were determined for the test compounds. In addition, the mechanism of inhibition of ATX-mediated FS3 hydrolysis was determined by varying the concentration of substrate (0.3–20 μM) in the presence of three concentrations of each inhibitor [0, 0.5× and 2×(IC_{50})]. Kinetic data including V_{max} and K_M were determined with Kaleida Graph 4.0 (version 4.03, Synergy Software, Reading, PA, USA) after the plots of initial velocities versus substrate concentration in the absence or presence of inhibitors were fit to the following equation: $y=m_1\times m_2\times x/(1+m_2\times x)$, in which $K_M=1/m_2$ and $V_{max}=m_1$. The average K_M value for ATX-mediated FS3 hydrolysis was determined to be 2.3 μM and was used in the following calculations. Simultaneous nonlinear regression using WinNonLin 6.1 (Pharsight, Mountain View, CA, USA) was used to assign the mechanism of inhibition.[36,37,39] K_i and K_i' values (affinities for free enzyme and the enzyme–substrate complex, respectively) were determined by calculating the lowest averaged percent residuals for each mechanism derived from curve fitting using the Michaelis–Menten equations for competitive, uncompetitive, mixed-mode, and noncompetitive inhibition.

Calcium mobilization assays

Assays for the mobilization of intracellular Ca^{2+} were performed as described.[44,57] Test compounds up to a final concentration of 10 μM either alone or mixed with respective ~EC_{50} concentrations of LPA 18:1 for each of LPAR subtype were added to cells stably expressing $LPA_{1,2,3,4,5}$, GPR87, and P2Y10 LPAR subtypes.[46] The cells were loaded with Fura-2/AM in Krebs buffer containing 0.001% pluronic acid for 1 h, and rinsed with Krebs buffer before measuring Ca^{2+} mobilization. The Ca^{2+} responses were measured by using a Flex Station II fluorescent plate reader (Molecular Devices, Sunnyvale, CA, USA). The ratio of peak emissions at $\lambda=510$ nm after 2 min of ligand addition was determined for excitation wavelengths of 340/380 nm. All samples were run in triplicate, and assays were performed at least twice for each receptor.

NPP6 and NPP7 inhibition assay

Inhibition of NPP6 and NPP7 was evaluated using recombinant purified proteins, the synthetic substrate *para*-nitrophenylphosphocholine (pNPPC), and a Synergy II plate reader (BioTek, Winooski, VT) as we have previously described.[36,39] The final concentration of each enzyme was 8.3 nM and pNPPC was 10 μM. All analogues were tested at single 10 μM concentrations. Absorbance of liberated *para*-nitrophenol at $\lambda=405$ nm was determined up to 1 h (where responses were linear) and was normalized to vehicle control.

MM1 hepatoma cell invasion of endothelial monolayers

The highly invasive MM1 cells originally isolated from the AH130 rat hepatoma cells were a kind gift from Dr. Michiko Mukai (Osaka University, Japan).[35,49] These cells were grown in suspension in Dulbecco's modified Eagle's medium (DMEM) supplemented with 10% fetal bovine serum (FBS), 2 mM glutamine, 100 U mL^{-1} penicillin, and 100 μg mL^{-1} streptomycin. The isolation and culture of mesothelial cells from C57BL/6 mice was previously described.[35,49] HUVECs obtained from VEC Technologies Inc. (Rensselaer, NY, USA) were grown in MCDB-131 complete medium containing 10% FBS, 90 μg mL^{-1} heparin, 10 ng mL^{-1} EGF, 1 μg mL^{-1} hydrocortisone, 0.2 mg mL^{-1} EndoGrowth supplement, 100 U mL^{-1} penicillin G, 100 μg mL^{-1} streptomycin, and 25 μg mL^{-1} amphotericin B (all from VEC Technologies). Tumor cell invasion was performed by seeding 1.3×10^5 HUVECs (passage 7) into each well of a 12-well plate precoated with 0.2% gelatin (Sigma) and cultured for two days to form a confluent monolayer. Mesothelial cells harvested from two to three mice were initially plated in six-well plates and grown to confluency in DMEM medium supplemented with 10% FBS in the presence of 100 U mL^{-1} penicillin G and 100 μg mL^{-1} streptomycin. When confluent, the mesothelial cells were split into three equal aliquots (~5×10^4 cells each) and plated to three wells of a 12-well plate and grown to confluence. For all invasion assays, MM1 cells were pre-stained with 2 μg mL^{-1} calcein AM (Invitrogen, USA) for 2 h, rinsed once, and seeded at a density of 5×10^4 cells per well over the monolayers. Tumor cells were left to invade the HUVEC monolayer for 24 h in MCDB-131 complete media containing 1% serum with or without addition of 1.5 μM LPC. MM1 cells were plated on the mesothelial monolayers in 2% FBS-supplemented DMEM in the presence of 100 U mL^{-1} penicillin G and 10 μg mL^{-1} streptomycin with or without 1.5 μM LPC (5 μM for the mesothelial cells), and invasion was allowed to proceed for 20 h. The day after MM1 cell seeding, non-invaded tumor cells were removed by five repeat rinses of the HUVEC monolayer (three rinses for the meso-

thelial monolayers) with PBS (containing Ca^{2+} and Mg^{2+}) followed by fixation with 10% buffered formalin. The number of tumor cells that penetrated the monolayer was photographed under a NIKON TiU inverted microscope using phase-contrast and fluorescence illumination in a minimum of five non-overlapping fields at 100× magnification. The fluorescent images were overlayed on the phase-contrast images using Elements BR software (version 3.1x), and the invaded MM1 cells showing the characteristic flattened morphology in the plane of focus underneath the monolayer were counted. For the invasion assay, LPC dissolved in chloroform was dried, re-dissolved in 1 mM charcoal-stripped BSA in PBS and added immediately to the HUVEC or mesothelium monolayer and co-cultured with MM1 cells with or without the ATX inhibitors. The final BSA concentration was 30 μM.

Acute murine toxicity studies

To determine acute toxicity of compound **22** we injected it at 1, 10, and 30 mg kg^{-1} day^{-1} doses intraperitoneally into groups of six adult Swiss mice for 10 days and monitored behavior and weight daily. The mice were sacrificed on day 14, and necropsies were conducted for signs of organ damage.

Pharmacokinetic studies

Studies were approved by the Institute of Animal Care and Use Committee (IACUC) of the University of Tennessee, Memphis. Animal treatment was in accordance with regulations outlined in the United States Department of Agriculture (USDA) Animal Welfare Act (9CFR, Parts 1, 2, and 3) and the conditions specified in the Guide for the Care and Use of Laboratory Animals. Male Sprague–Dawley rats (250–275 grams) pre-cannulated with jugular and femoral vein catheters were obtained from Charles River Laboratories (Wilmington, MA, USA). The patency of the jugular and femoral vein catheters was maintained every other day with heparinized glycerol solution (500 IU heparin per mL final solution in 50% glycerol) according to the vendor's instructions. Animals were fed a normal laboratory diet, allowed access to water ad libitum, and maintained on a 12 h light–dark cycle (25 °C).

Compound **22** was dissolved in propylene glycol and diluted in normal rat plasma. Rats were given a single intravenous (i.v.) bolus dose of compound **22** (5.8 mg kg^{-1}) via the femoral vein catheter. Blood (200 μL) was collected from the jugular vein catheter at timed intervals (5, 15, 30, 45, 60, 120, 240, 480, and 1440 min) into Microtainer brand tubes with lithium heparin (BD, Franklin Lakes, NJ, USA). Samples were centrifuged (10000 *g*, 25 °C) for 3 min, and the plasma was stored at −80 °C until analysis. Sample aliquots (50 μL) were mixed with 100 μL citrate phosphate buffer (30 mM citric acid, 40 mM Na_2HPO_4, pH 4.0), 400 μL water-saturated butanol, 200 ng internal standard (compound **10**), and 100 ng LPA 17:0. Samples were centrifuged (10000 *g*) for 1 min, and the butanol layer was transferred to a new tube and dried under argon gas. Plasma concentrations were determined similarly to a previously described method.[58] Compound **22** and LPA concentrations were determined by LC–MS–MS using an Applied Biosystems Sciex ABI 4000 QTRAP tandem mass spectrometer (Foster City, CA, USA) equipped with a Turboionspray™ interface, a Shimadazu LC-10ADvp HLPC pump (Columbia, MD, USA), and a Leap HTS PAL autosampler (Carrboro, NC, USA). Samples (5 μL) were injected onto a C_8 analytical column (Symmetry, 3.5 μm, 2.1 mm × 100 mm; Waters Corporation, Milford, MA, USA) with a solvent consisting of CH_3CN and H_2O containing 10 mM ammonium acetate using an isocratic flow rate of 0.3 mL min^{-1}.[59] The spectra were processed using Analyst software, version 1.5. The molecular species of LPA and compound **22** were analyzed by multiple reaction monitoring (MRM) in negative ion mode. The Q3 (product ion) was set at *m/z* 153.0 for LPA, 79.0 for compound **22**, and 186.0 for compound **10**. Q1 was set for the neutral molecular ion. Quantification was done by calculating the ratio of peak area to that of the appropriate internal standard.

Pharmacokinetic data analysis

Compound **22** plasma concentration–time data were analyzed by non-compartmental methods. The area under the plasma concentration–time curve from time 0 to infinity ($AUC_{0-\infty}$) was calculated by the trapezoidal rule with extrapolation to time infinity. The terminal half-life ($t_{1/2}$) was calculated as $0.693/\lambda_z$, for which λ_z is the terminal phase elimination constant. Plasma clearance (CL) was calculated as $CL = dose_{i.v.}/AUC_{i.v.0-\infty}$, where $dose_{i.v.}$ and $AUC_{i.v.0-\infty}$ are the i.v. dose and corresponding area under the curve from time 0 to infinity, respectively. The apparent volume of distribution at equilibrium (V_{dss}) was calculated as $V_{dss} = CL \times MRT$, where MRT is the mean residence time after the i.v. bolus dose. MRT was calculated as $MRT = (AUMC_{i.v.0-\infty})/(AUC_{i.v.0-\infty})$, where $AUMC_{i.v.0-\infty}$ is the area under the first moment of the plasma concentration–time curve extrapolated to infinity.

B16-F10 murine melanoma metastasis model

All animal procedures were approved by the Institutional Animal Care and Use Committee at the University of Tennessee and the M.D. Anderson Cancer Center and were consistent with the Guide for the Care and Use of Laboratory Animals (National Institutes of Health publication 85–23, revised 1985). Eight-week-old female C57BL/6 mice were injected with 5×10^4 cells per animal via tail veins and divided randomly into four groups. Each group then received selective ATX inhibitor (**22** or **30b**) or dual ATX and LPAR antagonist LPA-BP,[34] all at 0.5 mg kg^{-1} per injection, or vehicle (PBS with 1% DMSO) via intraperitoneal injection 30 min after the B16-F10 injection and daily for an additional 10 days. Subsequently, animals in all groups were monitored for another 10 days without treatment. At day 21, all mice were sacrificed and lungs were harvested, inflated, and fixed with 10% formalin. The number of metastatic nodules on the lung surface was counted. The number of lung nodules was compared against vehicle-treated group by one-way ANOVA followed by Newman–Keuls multiple comparison test and $p < 0.05$ was considered significant.

Acknowledgements

This work was supported by NIH-NCI CA 92160 (G.T.), the Van Vleet Oncology Research Fund (G.T.), the Breast Cancer Research Foundation (N.P.), and Lpath Inc. (G.B.M.).

Keywords: phosphonic acids · inhibitors · receptors · structure–activity relationships

[1] M. Umezu-Goto, Y. Kishi, A. Taira, K. Hama, N. Dohmae, K. Takio, T. Yamori, G. B. Mills, K. Inoue, J. Aoki, H. Arai, *J. Cell Biol.* **2002**, *158*, 227–233.

[2] A. Tokumura, E. Majima, Y. Kariya, K. Tominaga, K. Kogure, K. Yasuda, K. Fukuzawa, *J. Biol. Chem.* **2002**, *277*, 39436–39442.

[3] J. M. Wu, Y. Xu, N. J. Skill, H. Sheng, Z. Zhao, M. Yu, R. Saxena, M. A. Maluccio, *Mol. Cancer* **2010**, *9*, 71.
[4] M. A. Nouh, X. X. Wu, H. Okazoe, H. Tsunemori, R. Haba, A. M. Abou-Zeid, M. D. Saleem, M. Inui, M. Sugimoto, J. Aoki, Y. Kakehi, *Cancer Sci.* **2009**, *100*, 1631 – 1638.
[5] Y. Yang, L. Mou, N. Liu, M. S. Tsao, *Am. J. Respir. Cell Mol. Biol.* **1999**, *21*, 216 – 222.
[6] N. Samadi, C. Gaetano, I. S. Goping, D. N. Brindley, *Oncogene* **2009**, *28*, 1028 – 1039.
[7] S. Vidot, J. Witham, R. Agarwal, S. Greenhough, H. S. Bamrah, G. J. Tigyi, S. B. Kaye, A. Richardson, *Cell. Signalling* **2010**, *22*, 926 – 935.
[8] A. Masuda, K. Nakamura, K. Izutsu, K. Igarashi, R. Ohkawa, M. Jona, K. Higashi, H. Yokota, S. Okudaira, T. Kishimoto, T. Watanabe, Y. Koike, H. Ikeda, Y. Kozai, M. Kurokawa, J. Aoki, Y. Yatomi, *Br. J. Haematol.* **2008**, *143*, 60 – 70.
[9] C. G. Gaetano, N. Samadi, J. L. Tomsig, T. L. Macdonald, K. R. Lynch, D. N. Brindley, *Mol. Carcinog.* **2009**, *48*, 801 – 809.
[10] A. Kehlen, N. Englert, A. Seifert, T. Klonisch, H. Dralle, J. Langner, C. Hoang-Vu, *Int. J. Cancer* **2004**, *109*, 833 – 838.
[11] S. Liu, M. Umezu-Goto, M. Murph, Y. Lu, W. Liu, F. Zhang, S. Yu, L. C. Stephens, X. Cui, G. Murrow, K. Coombes, W. Muller, M. C. Hung, C. M. Perou, A. V. Lee, X. Fang, G. B. Mills, *Cancer Cell* **2009**, *15*, 539 – 550.
[12] M. Gugger, R. White, S. Song, B. Waser, R. Cescato, P. Riviere, J. C. Reubi, *Dis. Markers* **2008**, *24*, 41 – 50.
[13] H. Sakagami, J. Aoki, Y. Natori, K. Nishikawa, Y. Kakehi, Y. Natori, H. Arai, *J. Biol. Chem.* **2005**, *280*, 23084 – 23093.
[14] R. D. Duan, T. Bergman, N. Xu, J. Wu, Y. Cheng, J. Duan, S. Nelander, C. Palmberg, A. Nilsson, *J. Biol. Chem.* **2003**, *278*, 38528 – 38536.
[15] A. Nilsson, J. Wu, B. A. Jonsson, H. Stenstad, W. Agace, Y. Cheng, R. D. Duan, *Biochem. J.* **2006**, *394*, 299 – 308.
[16] M. Tanaka, S. Okudaira, Y. Kishi, R. Ohkawa, S. Iseki, M. Ota, S. Noji, Y. Yatomi, J. Aoki, H. Arai, *J. Biol. Chem.* **2006**, *281*, 25822 – 25830.
[17] L. A. van Meeteren, P. Ruurs, C. Stortelers, P. Bouwman, M. A. van Rooijen, J. P. Pradere, T. R. Pettit, M. J. Wakelam, J. S. Saulnier-Blache, C. L. Mummery, W. H. Moolenaar, J. Jonkers, *Mol. Cell. Biol.* **2006**, *26*, 5015 – 5022.
[18] S. Fotopoulou, N. Oikonomou, E. Grigorieva, I. Nikitopoulou, T. Paparountas, A. Thanassopoulou, Z. Zhao, Y. Xu, D. L. Kontoyiannis, E. Remboutsika, V. Aidinis, *Dev. Biol.* **2010**, *339*, 451 – 464.
[19] D. L. Baker, P. Morrison, B. Miller, C. A. Riely, B. Tolley, A. M. Westermann, J. M. Bonfrer, E. Bais, W. H. Moolenaar, G. Tigyi, *JAMA* **2002**, *287*, 3081 – 3082.
[20] R. Sutphen, Y. Xu, G. D. Wilbanks, J. Fiorica, E. C. Grendys, Jr., J. P. LaPolla, H. Arango, M. S. Hoffman, M. Martino, K. Wakeley, D. Griffin, R. W. Blanco, A. B. Cantor, Y. J. Xiao, J. P. Krischer, *Cancer Epidemiol. Biomarkers Prev.* **2004**, *13*, 1185 – 1191.
[21] Y. Xu, D. C. Gaudette, J. D. Boynton, A. Frankel, X. J. Fang, A. Sharma, J. Hurteau, G. Casey, A. Goodbody, A. Mellors, *Clin. Cancer Res.* **1995**, *1*, 1223 – 1232.
[22] I. Dimova, S. Raitcheva, R. Dimitrov, N. Doganov, D. Toncheva, *Eur. J. Cancer* **2006**, *42*, 674 – 679.
[23] N. Euer, M. Schwirzke, V. Evtimova, H. Burtscher, M. Jarsch, D. Tarin, U. H. Weidle, *Anticancer Res.* **2002**, *22*, 733 – 740.
[24] E. Shuyu, Y. J. Lai, R. Tsukahara, C. S. Chen, Y. Fujiwara, J. Yue, J. H. Yu, H. Guo, A. Kihara, G. Tigyi, F. T. Lin, *J. Biol. Chem.* **2009**, *284*, 14558 – 14571.
[25] A. A. Jazaeri, C. S. Awtrey, G. V. Chandramouli, Y. E. Chuang, J. Khan, C. Sotiriou, O. Aprelikova, C. J. Yee, K. K. Zorn, M. J. Birrer, J. C. Barrett, J. Boyd, *Clin. Cancer Res.* **2005**, *11*, 6300 – 6310.
[26] S. Tsuda, S. Okudaira, K. Moriya-Ito, C. Shimamoto, M. Tanaka, J. Aoki, H. Arai, K. Murakami-Murofushi, T. Kobayashi, *J. Biol. Chem.* **2006**, *281*, 26081 – 26088.
[27] L. A. van Meeteren, P. Ruurs, E. Christodoulou, J. W. Goding, H. Takakusa, K. Kikuchi, A. Perrakis, T. Nagano, W. H. Moolenaar, *J. Biol. Chem.* **2005**, *280*, 21155 – 21161.
[28] G. G. Durgam, R. Tsukahara, N. Makarova, M. D. Walker, Y. Fujiwara, K. R. Pigg, D. L. Baker, V. M. Sardar, A. L. Parrill, G. Tigyi, D. D. Miller, *Bioorg. Med. Chem. Lett.* **2006**, *16*, 633 – 640.
[29] H. M. Albers, L. A. van Meeteren, D. A. Egan, E. W. van Tilburg, W. H. Moolenaar, H. Ovaa, *J. Med. Chem.* **2010**, *53*, 4958 – 4967.
[30] H. M. Albers, A. Dong, L. A. van Meeteren, D. A. Egan, M. Sunkara, E. W. van Tilburg, K. Schuurman, T. O. van, A. J. Morris, S. S. Smyth, W. H. Moolenaar, H. Ovaa, *Proc. Natl. Acad. Sci. USA* **2010**, *107*, 7257 – 7262.
[31] D. L. Baker, Y. Fujiwara, K. R. Pigg, R. Tsukahara, S. Kobayashi, H. Murofushi, A. Uchiyama, K. Murakami-Murofushi, E. Koh, R. W. Bandle, H. S. Byun, R. Bittman, D. Fan, M. Murph, G. B. Mills, G. Tigyi, *J. Biol. Chem.* **2006**, *281*, 22786 – 22793.
[32] J. Gajewiak, R. Tsukahara, Y. Fujiwara, G. Tigyi, G. D. Prestwich, *Org. Lett.* **2008**, *10*, 1111 – 1114.
[33] J. Gajewiak, R. Tsukahara, T. Tsukahara, Y. Fujiwara, S. Yu, Y. Lu, M. Murph, G. B. Mills, G. Tigyi, G. D. Prestwich, *ChemMedChem* **2007**, *2*, 1789 – 1798.
[34] H. Zhang, X. Xu, J. Gajewiak, R. Tsukahara, Y. Fujiwara, J. Liu, J. I. Fells, D. Perygin, A. L. Parrill, G. Tigyi, G. D. Prestwich, *Cancer Res.* **2009**, *69*, 5441 – 5449.
[35] A. Uchiyama, M. Mukai, Y. Fujiwara, S. Kobayashi, N. Kawai, H. Murofushi, M. Inoue, S. Enoki, Y. Tanaka, T. Niki, T. Kobayashi, G. Tigyi, K. Murakami-Murofushi, *Biochim. Biophys. Acta* **2007**, *1771*, 103 – 112.
[36] A. B. Hoeglund, H. E. Bostic, A. L. Howard, I. W. Wanjala, M. D. Best, D. L. Baker, A. L. Parrill, *J. Med. Chem.* **2010**, *53*, 1056 – 1066.
[37] A. B. Hoeglund, A. L. Howard, I. W. Wanjala, T. C. Pham, A. L. Parrill, D. L. Baker, *Bioorg. Med. Chem.* **2010**, *18*, 769 – 776.
[38] E. J. North, D. A. Osborne, P. K. Bridson, D. L. Baker, A. L. Parrill, *Bioorg. Med. Chem.* **2009**, *17*, 3433 – 3442.
[39] E. J. North, A. L. Howard, I. W. Wanjala, T. C. Pham, D. L. Baker, A. L. Parrill, *J. Med. Chem.* **2010**, *53*, 3095 – 3105.
[40] A. L. Parrill, *Biochim. Biophys. Acta* **2008**, *1781*, 540 – 546.
[41] A. L. Parrill, D. L. Baker, *Anticancer Agents Med. Chem.* **2008**, *8*, 917 – 923.
[42] G. Ferry, N. Moulharat, J. P. Pradere, P. Desos, A. Try, A. Genton, A. Giganti, M. Beucher-Gaudin, M. Lonchampt, M. Bertrand, J. S. Saulnier-Blache, G. C. Tucker, A. Cordi, J. A. Boutin, *J. Pharmacol. Exp. Ther.* **2008**, *327*, 809 – 819.
[43] Y. C. Kim, S. G. Brown, T. K. Harden, J. L. Boyer, G. Dubyak, B. F. King, G. Burnstock, K. A. Jacobson, *J. Med. Chem.* **2001**, *44*, 340 – 349.
[44] G. Jiang, Y. Xu, Y. Fujiwara, T. Tsukahara, R. Tsukahara, J. Gajewiak, G. Tigyi, G. D. Prestwich, *ChemMedChem* **2007**, *2*, 679 – 690.
[45] W. J. Valentine, G. N. Kiss, J. Liu, E S, M. Gotoh, K. Murakami-Murofushi, T. C. Pham, D. L. Baker, A. L. Parrill, X. Lu, C. Sun, R. Bittman, N. J. Pyne, G. Tigyi, *Cell. Signalling* **2010**, *22*, 1543 – 1553.
[46] J. R. Williams, A. L. Khandoga, P. Goyal, J. I. Fells, D. H. Perygin, W. Siess, A. L. Parrill, G. Tigyi, Y. Fujiwara, *J. Biol. Chem.* **2009**, *284*, 17304 – 17319.
[47] F. Imamura, T. Horai, M. Mukai, K. Shinkai, H. Akedo, *Jpn. J. Cancer Res.* **1991**, *82*, 493 – 496.
[48] F. Imamura, T. Horai, M. Mukai, K. Shinkai, M. Sawada, H. Akedo, *Biochem. Biophys. Res. Commun.* **1993**, *193*, 497 – 503.
[49] M. Mukai, F. Imamura, M. Ayaki, K. Shinkai, T. Iwasaki, K. Murakami-Murofushi, H. Murofushi, S. Kobayashi, T. Yamamoto, H. Nakamura, H. Akedo, *Int. J. Cancer* **1999**, *81*, 918 – 922.
[50] M. Mukai, H. Nakamura, M. Tatsuta, T. Iwasaki, A. Togawa, F. Imamura, H. Akedo, *FEBS Lett.* **2000**, *484*, 69 – 73.
[51] N. Watanabe, H. Ikeda, K. Nakamura, R. Ohkawa, Y. Kume, T. Tomiya, K. Tejima, T. Nishikawa, M. Arai, M. Yanase, J. Aoki, H. Arai, M. Omata, K. Fujiwara, Y. Yatomi, *Life Sci.* **2007**, *81*, 1009 – 1015.
[52] N. Watanabe, H. Ikeda, K. Nakamura, R. Ohkawa, Y. Kume, J. Aoki, K. Hama, S. Okudaira, M. Tanaka, T. Tomiya, M. Yanase, K. Tejima, T. Nishikawa, M. Arai, H. Arai, M. Omata, K. Fujiwara, Y. Yatomi, *J. Clin. Gastroenterol.* **2007**, *41*, 616 – 623.
[53] M. K. Altman, V. Gopal, W. Jia, S. Yu, H. Hall, G. B. Mills, A. C. McGinnis, M. G. Bartlett, G. Jiang, D. Madan, G. D. Prestwich, Y. Xu, M. A. Davies, M. M. Murph, *Mol. Cancer* **2010**, *9*, 140.
[54] J. Gierse, A. Thorarensen, K. Beltey, E. Bradshaw-Pierce, L. Cortes-Burgos, T. Hall, A. Johnston, M. Murphy, O. Nemirovskiy, S. Ogawa, L. Pegg, M. Pelc, M. Prinsen, M. Schnute, J. Wendling, S. Wene, R. Weinberg, A. Wittwer, B. Zweifel, J. Masferrer, *J. Pharmacol. Exp. Ther.* **2010**, *334*, 310 – 317.
[55] G. D. Prestwich, Y. Xu, L. Qian, J. Gajewiak, G. Jiang, *Biochem. Soc. Trans.* **2005**, *33*, 1357 – 1361.
[56] S. Jansen, M. Andries, K. Vekemans, H. Vanbilloen, A. Verbruggen, M. Bollen, *Cancer Lett.* **2009**, *284*, 216 – 221.

[57] G. G. Durgam, T. Virag, M. D. Walker, R. Tsukahara, S. Yasuda, K. Liliom, L. A. van Meeteren, W. H. Moolenaar, N. Wilke, W. Siess, G. Tigyi, D. D. Miller, *J. Med. Chem.* **2005**, *48*, 4919 – 4930.
[58] H. Kosanam, F. Ma, H. He, S. Ramagiri, V. Gududuru, G. J. Tigyi, R. K. Van, D. D. Miller, C. R. Yates, *J. Chromatogr. B* **2010**, *878*, 2379 – 2383.
[59] A. Tokumura, L. D. Carbone, Y. Yoshioka, J. Morishige, M. Kikuchi, A. Postlethwaite, M. A. Watsky, *Int. J. Med. Sci.* **2009**, *6*, 168 – 176.

Received: October 4, 2010
Revised: February 21, 2011
Published online on April 4, 2011

